

Methods for Engine Supervision and Control based on Cylinder Pressure Information

Steffen Leonhardt, Norbert Müller and Rolf Isermann

Darmstadt University of Technology

Institute of Automatic Control

Landgraf-Georg-Str. 4

D-64283 Darmstadt, Germany

Tel. (+49) 6151-16 23 07

Fax. (+49) 6151-29 34 45

email: {sleonhardt, nmueller, risermann}@iat.tu-darmstadt.de

Keywords: Cylinder Pressure, Neural Networks, Failure detection, Online Learning

Abstract

The increasing demand for low emissions and low fuel consumption in modern combustion engines require improved methods for on-line diagnosis and optimal control of the combustion process. In this paper, it will be demonstrated that the cylinder pressure signal can successfully be used for this task. After introduction of some theoretical background, several application examples are presented: an on-line supervision of fuel injection, some results on feedforward emission control and a concept for feedback control of spark timing. Experimental results obtained from stock car diesel and Spark Ignition (SI) engines are included to support the automation concepts.

1 Introduction

Cylinder pressure measurements have a long history. Until the early fifties, pressure measurements were only possible in steady state and the obtained data was mainly used for design purpose and combustion analysis. The development of *electronic* pressure sensors and the progress in off-line computation power made the cylinder

pressure analysis a common tool in modern combustion engine design [2, 12].

During the last few years, real-time engine control and on-board supervision based on cylinder pressure information have become of particular interest. This is mainly due to the availability of cost-effective cylinder pressure sensors, whose durability are expected to meet vehicle life-time [1, 11]. First applications in commercial cars have been reported in [15] and [14], where cylinder pressure sensors have been used for ignition control and for lean combustion engine control, respectively. Since other sensors like the needle stroke sensor, the knock sensor or the air-mass meter could be replaced, the resulting financial burden appears not as a major problem anymore [10, 24].

Using real-time combustion pressure measurements as a feedback signal offers a variety of potential advantages [23]. For example, closed loop *spark timing control* aims at optimal injection timing in the presence of changing engine and environmental conditions. In SI engines, another application is *knock detection*. The sensors currently used for this task are known to be sensitive to ambient noise, especially at high engine speeds [1]. Indeed, using a cylinder pressure sensor instead

allows to operate the engine close to the detonation limit, thus improving fuel economy and performance. One manufacturer has reported power improvements of 7 to 15 % [24].

Regarding control of fuel mixture in SI engines, several control application can be found in the literature. For *lean-burn control*, statistical fluctuations between successive combustion cycles can be monitored and allow to safely operate each cylinder at its individual lean limit [14]. The same approach can be used for *exhaust gas recirculation (EGR) control*, where maximization of EGR ratio close to the misfire limit can be used for emission reduction [11]. By contrast, stoichiometric *air-fuel ratio* control can be performed by extracting characteristic features from the pressure traces in combination with a calibration procedure [6]. This allows air-fuel closed-loop control also during warm-up.

Upcoming and future exhaust norms motivate special interest in *engine monitoring* and *fault diagnosis* of the compression, injection, ignition and fuel delivery systems. For example, *misfire detection* is currently performed by monitoring the fly-wheel speed signal. At high engine speeds or low engine loads, this approach suffers from a poor signal to noise ratio. The on-line analysis of the cylinder pressure signal is one of the most promising approaches to substitute the fly-wheel speed analysis.

The relations between engine input signals like fuel mass and injection point (ignition point for SI engines) and exhaust emissions have been studied for a long time. For SI engines, Nitzschke has already shown that exhaust emissions are individual events without dynamics from rotation to rotation [22]. Therefore, using the cylinder pressure for *feedforward control* of the individual exhaust production is very likely to improve overall exhaust emissions, especially in transient operation.

2 Methods for Cylinder Pressure Analysis

To control or monitor the condition of the engine, a real-time analysis of the combustion heat curve, i.e. the transformed energy per rotation angle, would be desirable. Referring to first principles, the equation of combustion can be written as

$$dQ_{hr} = dW + dU_s + dQ_w \quad (1)$$

where dQ_{hr} refers to gross heat energy released due to combustion, dW denotes the mechanical work due to piston movement and dU_s and dQ_w denote change in sensible internal energy and heat transfer from charge to cylinder wall, respectively [5]. Note that mass changes due to piston ring blow-by, valve leakage and fuel injection into the cylinder are ignored. However, for evaluating eq. (1), real-time conditions are difficult to match due to high computational costs. For on-line applications, an adequate pressure signal analysis is a more promising approach.

At Stanford University, Powell and co-workers have used the Location of cylinder Peak Pressure (LPP) for closed-loop spark timing in SI engines, see [13]. However, these early attempts had difficulties when the combustion charge was highly dilute or the engine was under light load [8, 20]. Another approach has been to use momentums of the pressure signal defined by

$$M_k = \int_{180}^{540} p_{cyl}(\theta) \theta^k d\theta \quad (2)$$

where θ corresponds to the crankshaft angle and k is an arbitrary integer, see [6, 7, 23].

Other groups have introduced competing concepts. At General Motors, Matekunas [20] proposed to consider *pressure ratios* while at Darmstadt University of Technology, Leonhardt introduced the *difference pressure* method, [16]. Both concepts are well suited for real-time applications

and will be discussed more detailed below. However, both concepts require an approximation of the "motored" pressure curve, which will now be introduced.

2.1 Approximation of the Motored Pressure

A physically motivated approach assumes a polytropic compression and calculates the reconstructed motored pressure at a specific crank angle θ by

$$p_{cyl,motored}(\theta) = p_{ref} \cdot \left(\frac{V_{ref}}{V_{cyl}(\theta)} \right)^\kappa \quad (3)$$

where V_{cyl} and κ refer to the cylinder volume and to the polytropic index, respectively. Since there always is an inevitable sensor offset, the absolute pressure p_{ref} has to be calculated at a predefined crank angle (i.e. a predefined cylinder volume V_{ref}). This can be done by evaluating eq. (3) for two different pressure samples during the compression stroke [12]. The precision and robustness of absolute pressure calculations can be improved by using more than two samples of the compression stroke and by applying a least squares fit [7].

A computationally less demanding approach developed by the authors is based on a numerical function approximation. For approximation of the motored pressure, the cylinder pressure signal prior to injection is reflected around TDC

$$p_{cyl,motored}(-\theta) = p_{cyl,measured}(\theta) \quad (4)$$

for $-180 \text{ deg} < \theta < \theta_{IN}$, where θ_{IN} refers to the angle of injection. Note that $p_{cyl,motored}(\theta) = p_{cyl,measured}(\theta)$ for $\theta < \theta_{IN}$. The missing curve segment is filled by a numerical function approximation

$$p_{cyl,motored}(\theta) = a |\theta|^{1.5} + b \quad (5)$$

for $|\theta| < |\theta_{IN}|$. A small ignition delay (ID) resulting in $\theta'_{IN} = \theta_{ID} + \theta_{IN}$ may be included. The

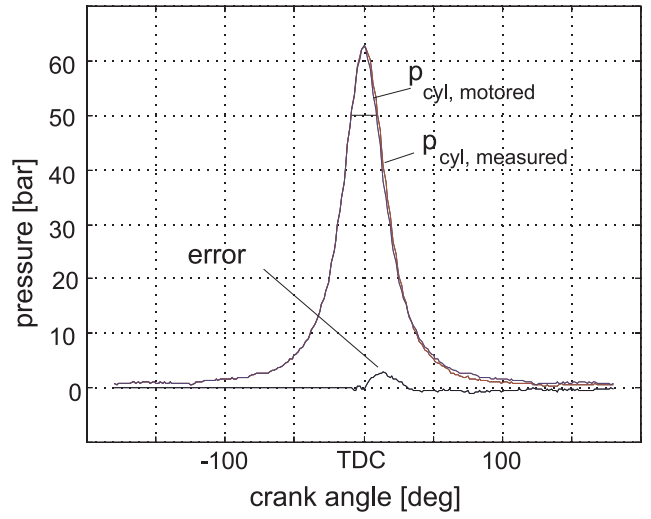


Figure 1: Reconstructed motored pressure and measured pressure in a diesel engine. $m_F = 0 \text{ mg}$, $n = 2400 \text{ rpm}$, approximation error $< 5 \%$

parameters a and b are estimated on-line by a least squares fit. Figure 1 shows the result. Note that this second method is independent of any pressure sensor offset.

2.2 The Difference Pressure

Only the difference pressure Δp_{cyl} carries information on the combustion and thus on the input variables fuel mass m_F and injection angle θ_{IN} ¹. In order to calculate Δp_{cyl} , the computed motored pressure signal must be subtracted from the fired cylinder pressure signal

$$\Delta p_{cyl}(\theta) = p_{cyl,fired}(\theta) - p_{cyl,motored}(\theta) \quad (6)$$

Figure 2 shows the result.

2.3 The Pressure Ratio Approach

The energy conversion during a combustion cycle can be described by the Mass Fraction Burned

¹In a signal theoretical sense, using Δp_{cyl} instead of p_{cyl} results in a contrast amplification

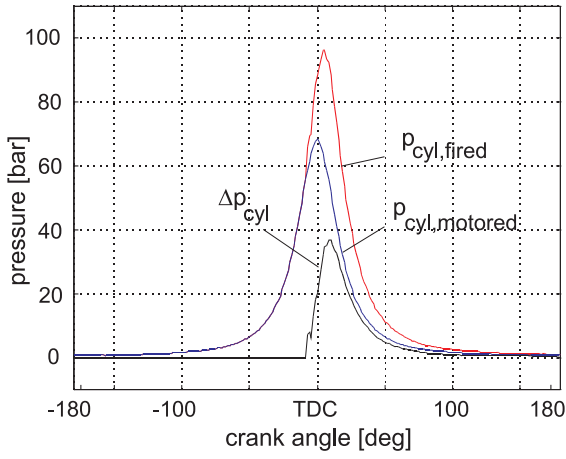


Figure 2: Cylinder pressure curves of a diesel engine, fuel mass $m_F = 10$ mg, injection angle $\theta_{IN} = 16$ deg, 2400 rpm

(MFB), see [20], which can be approximated by

$$\text{MFB}(\theta) \approx \frac{p_{\text{cyl},\text{fired}}(\theta)}{p_{\text{cyl},\text{motored}}(\theta)} - 1 \quad (7)$$

Figure 3 illustrates the motored and fired pressures during a combustion cycle, as well as MFB. Considering eq. (6) and (3), this equation can

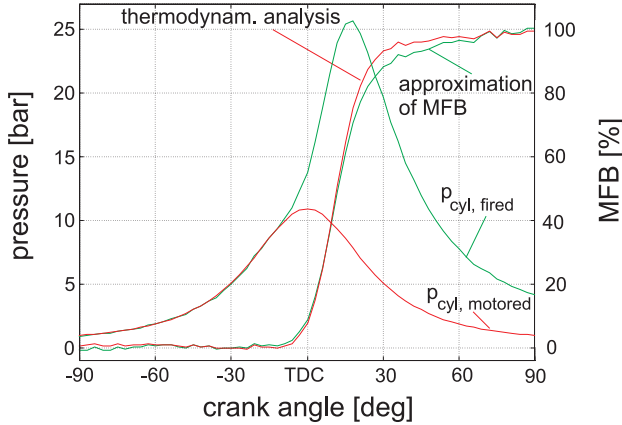


Figure 3: Fired and motored (polytrope) cylinder pressure signals and approximation of MFB in a SI engine

be interpreted as a weighted difference pressure

$$\begin{aligned} \text{MFB}(\theta) &\approx \frac{\Delta p_{\text{cyl}}(\theta)}{p_{\text{cyl},\text{motored}}(\theta)} \\ &= \frac{\Delta p_{\text{cyl}}(\theta)}{p_{\text{ref}}} \left(\frac{V_{\text{cyl}}(\theta)}{V_{\text{ref}}} \right)^\kappa \end{aligned} \quad (8)$$

Note that in Figure 3, the approximation of MFB as calculated by eq. (7) is in good accordance to a thermodynamic analysis as given in [12]. Note further that eq. (8) again reveals the dependency of this approach on a precise measurement of p_{ref} , see Section 2.1.

3 RBF Networks

Neural networks are known to be a valuable tool for approximation of nonlinear mappings [19], and may therefore be used for identification and control of nonlinear dynamic systems.

In the following, a short introduction to design and learning algorithms for Radial Basis Function (RBF) networks is given.

3.1 Structure of RBF Networks

A RBF network as shown in Figure 4 is defined as a linear combination of radial basis functions

$$y(\underline{x}) = \sum_{i=1}^M w_i \Phi_i(\underline{x}, \underline{c}_i, \sigma_i) \quad (9)$$

where w_i denote the output weights associated with each of the M basis functions Φ_i . $\underline{x} = [x_1 \ x_2 \ \dots \ x_n]^T$ is the input vector, $\underline{c}_i = [c_{i1} \ c_{i2} \ \dots \ c_{in}]^T$ are the vectors of the center coordinates of the M basis functions, and σ_i denote the widths of the basis functions. A very popular choice for the radial basis function is the Gaussian

$$G_i(\underline{x}, \underline{c}_i, \sigma_i) = \exp \left(-\frac{1}{2} \left(\frac{(x_1 - c_{i1})^2}{\sigma_i^2} + \frac{(x_2 - c_{i2})^2}{\sigma_i^2} + \dots + \frac{(x_n - c_{in})^2}{\sigma_i^2} \right) \right) \quad (10)$$

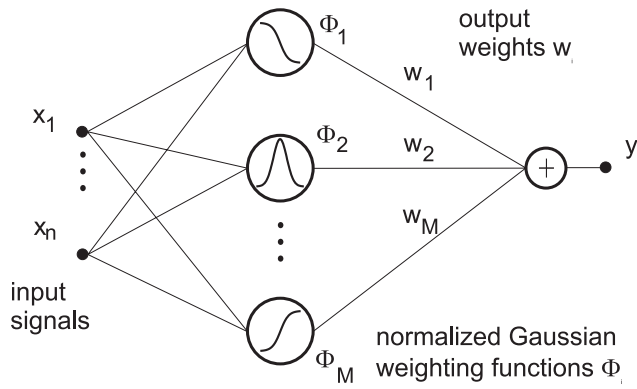


Figure 4: Radial basis function network with n input nodes, M normalized Gaussians and one output node

which was used here in its normalized form:

$$\Phi_i(\underline{x}, \underline{c}_i, \sigma_i) = \frac{G_i}{\sum_{j=1}^M G_j}. \quad (11)$$

Due to this normalization, the neural network forms a partition of unity which improves the interpolation properties and makes the network less sensitive to the choice of the widths σ_i , see [25].

3.2 Learning Algorithms

In eq. (9) three different kinds of parameters appear: the weights w_i , the centers coordinates \underline{c}_i , and the standard deviations σ_i . First, the centers and the standard deviations have to be fixed, which is usually done by some heuristic approach. Common algorithms for center determination are lattice methods, clustering or direct placement on the input data. Clustering methods ([3, 21]) place neurons only in those regions where data is present. The standard deviations can then be chosen by the nearest neighbor method, i.e. proportional to the distance to the nearest neighbor center [21]. The weight parameters w_i can be computed by

$$\underline{w} = (\underline{X}^T \underline{X})^{-1} \underline{X}^T \underline{y} \quad (12)$$

where the $(N \times M)$ matrix \underline{X} contains the weighted input signals. $\underline{y} = [y(1) \ y(2) \ \dots \ y(N)]^T$ contains

the process output signal for N training data samples. Since no nonlinear optimization technique is involved, fast training times can be achieved.

For on-line learning, a training algorithm, which can be applied during regular operation has been developed. For local tuning of the neuron weights, a simple yet computationally efficient learning algorithm, the Normalized Least Mean Squares (NLMS) rule as given by [4]

$$w_i^{\text{new}} = w_i^{\text{old}} + \mu \cdot e(\underline{x}) \cdot \frac{\Phi_i(\underline{x})}{\sum_{j=1}^M \Phi_j^2(\underline{x})} \quad (13)$$

was employed. Here, $e(\underline{x})$ denotes the error between the correct value and the old network output. μ represents the learning rate, which must be within the range $0 < \mu < 2$. However, appropriate values vary between 1 for fast learning and $\mu \ll 1$ for robustness against measurement noise.

4 Applications

4.1 Supervision of the Fuel Injection of a Diesel Engine

From a *control engineering viewpoint*, a Diesel engine has two inputs: the injected fuel mass m_F and the injection angle θ_{IN} . The torque T_{dyn} , the soot and the exhaust gases represent output signals. Engine variables like the cylinder pressure p_{cyl} , the cylinder temperature T_{cyl} , the turbo charger variables p_i and T_i and the oil temperature are referred to as internal states. The engine speed n is a function of torque and load and thus not an independent variable.

Internally, the engine can be separated into 4 blocks : the injection pump, the combustion dynamics, the thermodynamic block and the kinematics. Figure 5 gives a block diagram of a typical diesel engine including specific maps used for speed control and boost pressure limitation. By reconstruction of the input signals m_F and θ_{IN}

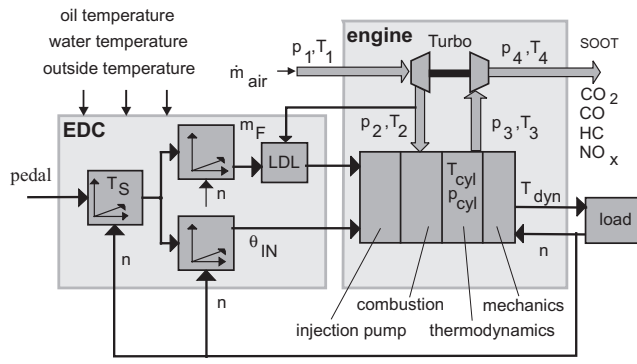


Figure 5: Structure of a typical car diesel engine with turbo-charger (EDC = Electronic Diesel Control, LDL = Load Dependent Boost Pressure Limitation)

from difference pressure features, the proper functioning of the fuel injection pump can be monitored. Injection faults can be detected by comparison with the desired reference values, Figure 6. The reconstruction of m_F and θ_{IN} from the dif-

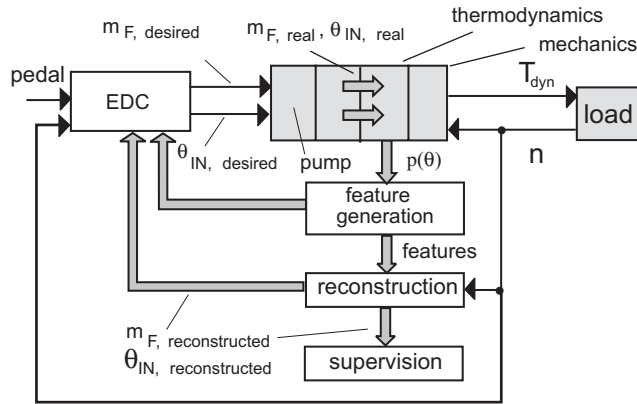


Figure 6: Concept for injection monitoring

ference pressure features can be interpreted as a nonlinear mapping. In order to approximate this mapping, an RBF network with 112 neurons was used and trained according to eq. (12) with reference values obtained from a dynamic engine test stand [17].

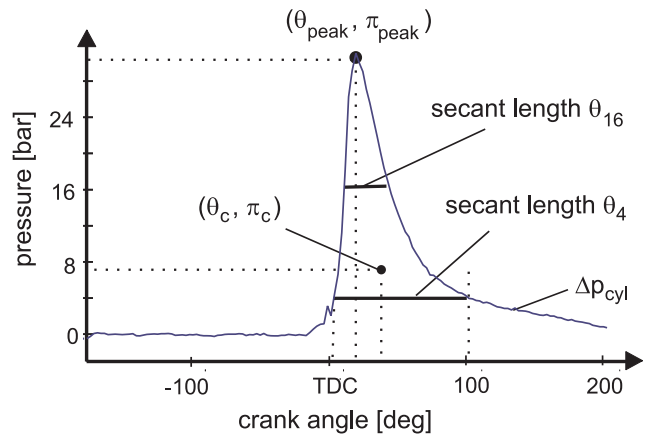


Figure 7: $\Delta p_{cyl}(\theta)$ and extracted features

4.1.1 Feature Extraction

For data reduction purposes, Δp_{cyl} needs to be characterized by numerical values. As shown in Figure 7, several features come to mind:

- the center of gravity (θ_c, π_c)

$$\theta_c = \frac{BDC}{BDC} \frac{\int_{BDC} \theta \Delta p d\theta}{\int_{BDC} \Delta p d\theta}, \pi_c = \frac{BDC}{BDC} \frac{\int_{BDC} \Delta p^2 d\theta}{\int_{BDC} \Delta p d\theta} \quad (14)$$

- the difference pressure peak $(\theta_{peak}, \pi_{peak})$
- the secant length θ_i

$$\theta_i = \theta_{max,i} - \theta_{min,i} \quad (15)$$

for $\Delta p_{cyl}(\theta_i) \geq \Delta p_{cyl,i}$ with $i = 4, 10, 16, \dots$

To investigate the dependency of the features on m_F and θ_{IN} , the input signals were varied both experimentally and in a combustion process simulation [16]. Figure 8 gives the simulation results at a specific operation point. As can be seen from Figure 9, the experimental results were quite similar indicating that (π_c, θ_c) are indeed unique nonlinear functions of m_F and θ_{IN} . For $(\pi_{peak}, \theta_{peak})$ and the secant lengths, similar results were obtained. Note that all features mentioned above

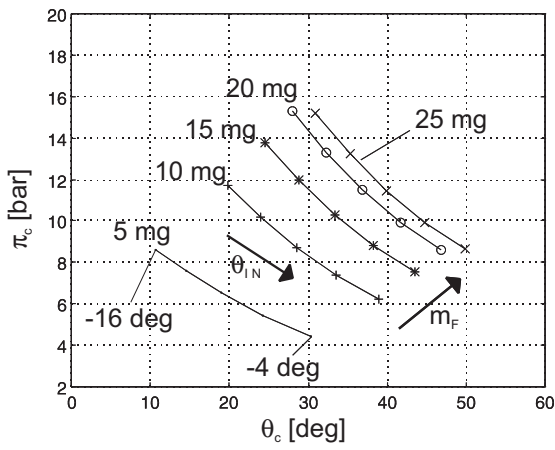


Figure 8: Map of (π_c, θ_c) , simulation, 2100 rpm

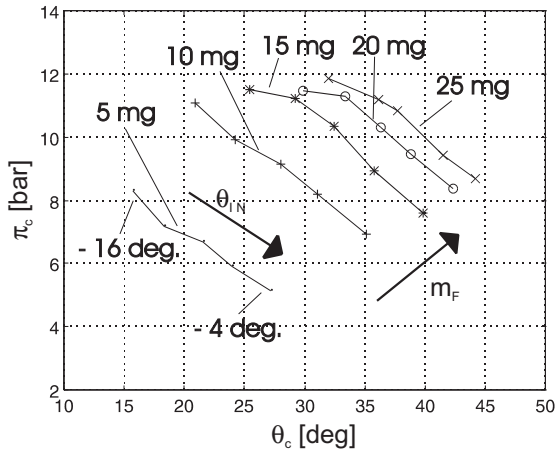


Figure 9: Map of (π_c, θ_c) , experiments, 2100 rpm

proved to vary uniquely with the input signals. Furthermore, all features have a dependency on the engine speed n , which can be shown both experimentally and by simulation, see [16].

4.1.2 Stationary Operation

Figure 10 shows some reconstruction results for m_F and θ_{IN} at different engine speeds. Here, the line length between + and \circ indicates the approximation error which was found to be generally less than 10 %.

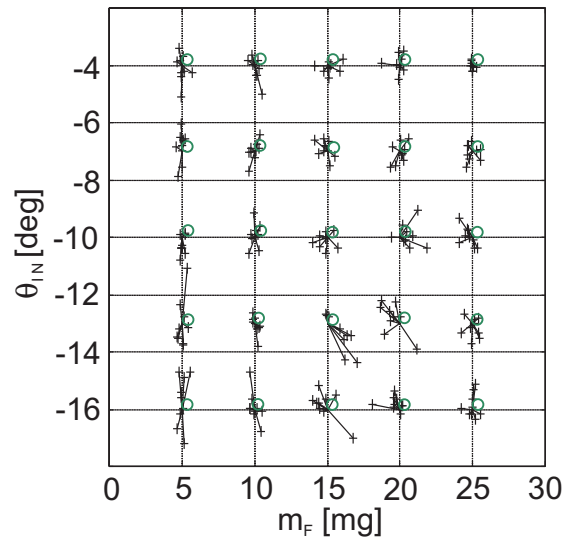


Figure 10: Reconstruction performance in the stationary case (9 engine speeds, \circ reference, + reconstructed value)

4.1.3 Dynamic Operation

As an example of reconstruction performance during dynamic engine operation, a (moderate) acceleration including gear shifting from 1st up to 5th gear is presented in Figures 11 and 12. Note that

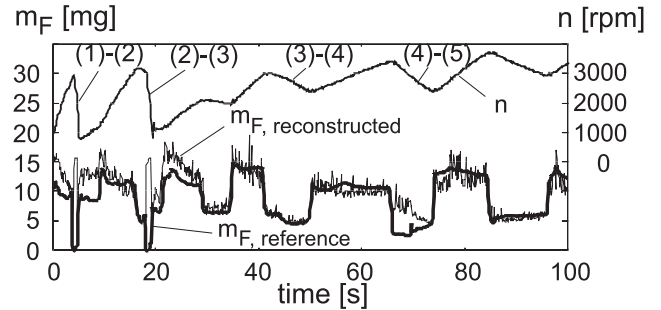


Figure 11: Reconstruction of injected fuel mass m_F during an acceleration maneuver (numbers in brackets indicate the actual gear)

during gear shift, fuel mass reconstruction was poor due to the fact that $m_F = 0$ was not included in the reference data set and therefore could not be reconstructed by the RBF network.

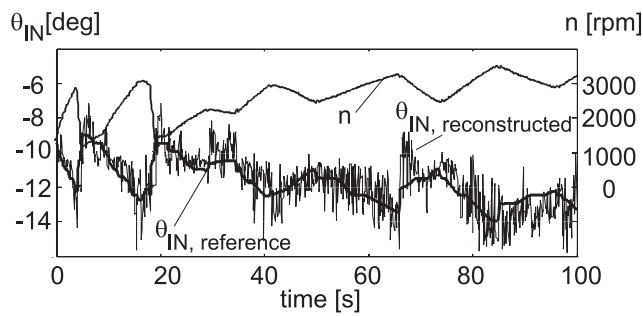


Figure 12: Reconstruction of injection angle θ_{IN} during an acceleration maneuver

4.1.4 Injection Fault Detection

As indicated in Figure 6, supervision and injection fault detection can be implemented by comparison of the reconstructed signals with the reference values. A simple and straightforward approach is to implement thresholds, Figure 13. These results

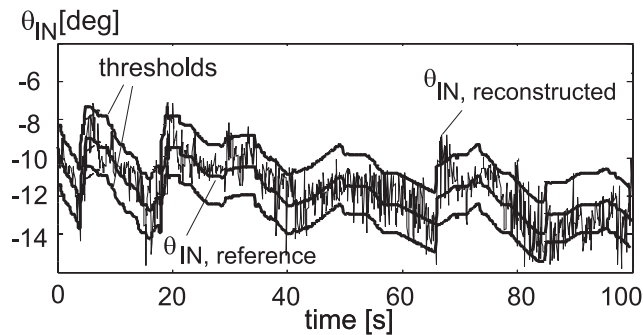


Figure 13: Concept for supervision of the injection (fixed thresholds of ± 1.5 deg. for θ_{IN}).

can be further improved by filtering² and by application of more advanced strategies like adaptive thresholds, etc..

²An on-line filtering would result in a smaller threshold bandwidth, but may also slow down reaction time

4.2 Feed-forward Control of Engine Output Signals

4.2.1 Input - Output Relations

In a whirl-chamber Diesel engine, the torque production basically is a function of the injected fuel mass, Figure 14. Indeed, while the shape of Δp_{cyl}

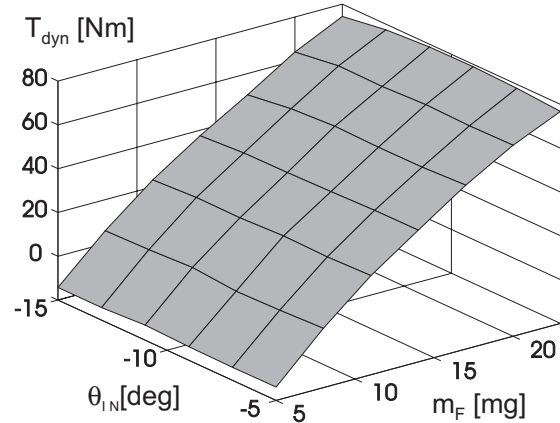


Figure 14: Engine torque as a function of m_F and θ_{IN} , 2500 rpm

changes significantly with θ_{IN} (see Figure 9), the injection angle only has a minor effect on torque production. This, however, is totally different when soot and exhaust production are considered. From a theoretical viewpoint, the formation of soot results from a lack of air. Therefore, the soot emissions³ are expected to increase as the "air-to-fuel" (A/F) ratio⁴ approaches 1. Indeed, the experimental results showed a strong influence of m_F and θ_{IN} on soot production, see Figure 15. In Diesel engines, the CO emissions generally behave similar to the soot production and increase with load, but in addition they should have a minimum for partial load. As shown in Figure 16, this was found to be true. Similar to the soot production, the CO emissions were influenced by both

³It is common practice to use the turbidity of the exhaust gases as an indicator for soot formation

⁴Remember that λ is defined as $\lambda = m_{air}/m_{air,stoichiometric}$ and that $\lambda = 1$ corresponds to an air-to-fuel ratio of 14.8 kg air/kg fuel

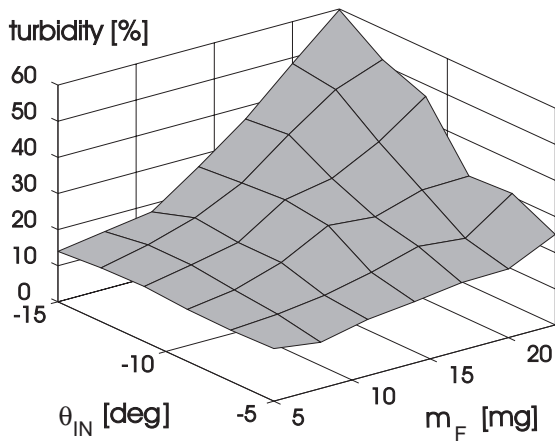


Figure 15: turbidity as a function of m_F and θ_{IN} , 2500 rpm (measured with a SICK DM61 sensor)

m_F and θ_{IN} . Nitrogen oxides result from high

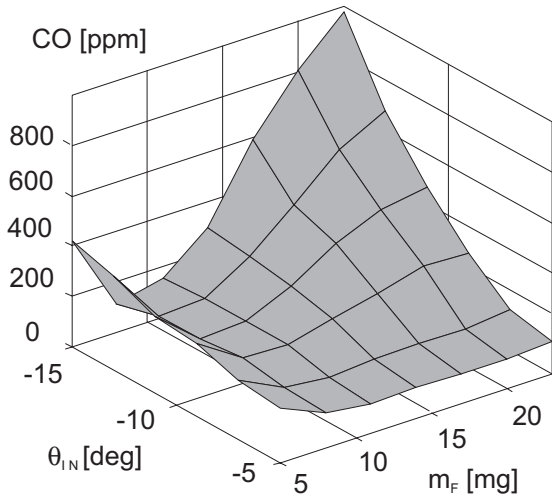


Figure 16: CO emissions as a function of m_F and θ_{IN} , 2500 rpm

cylinder temperatures during combustion. Figure 17 shows measurements obtained from the engine test stand. Note that the NO emissions have a maximum at very early injection angles. A similar effect was found for NO_2 and HC emissions, see [18]. This may be explained by the fact that early injection results in higher cylinder pressures and temperatures leading to higher NO_x production.

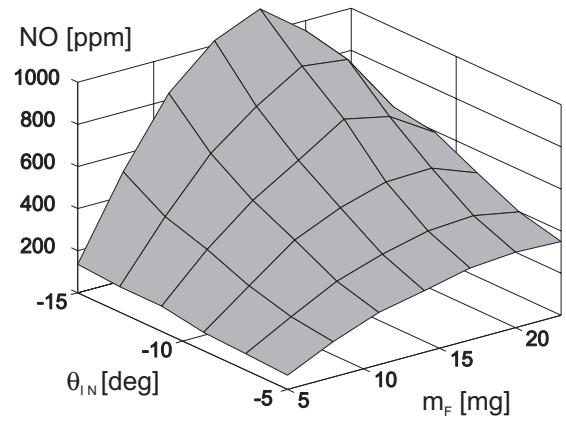


Figure 17: NO emissions as a function of m_F and θ_{IN} , 2500 rpm (measured with a BINOS sensor)

4.2.2 Relation between Cylinder Pressure and Output Signals

To control torque and exhaust emissions by analysis of the cylinder pressure, one requirement are unique relations between $\Delta p_{cyl}(\theta)$ and the output signals. In the following, this shall be demonstrated for θ_c and π_c , but since there are similar relationships for the other features, it is possible to use θ_{peak} and π_{peak} or the secant lengths as well. As shown in Figure 9, the mapping from m_F and θ_{IN} to θ_c and π_c is bijective. Thus, Figures 14 ... 17 can be displayed as functions of the center of gravity of $\Delta p_{cyl}(\theta)$ without loss of information. Figure 18 gives the torque signal while Figure 19 shows the corresponding turbidity signals. In Figures 20 and 21, the CO and the NO emissions are given as functions of θ_c and π_c .

4.2.3 Concept of pressure based feedforward control

It should be pointed out that there are unique non-linear relations between engine torque and exhaust emissions (*outputs*), and Δp_{cyl} (*internal states*).

Since the difference pressure signal carries the complete information of the torque production and the current exhaust emissions and since ex-

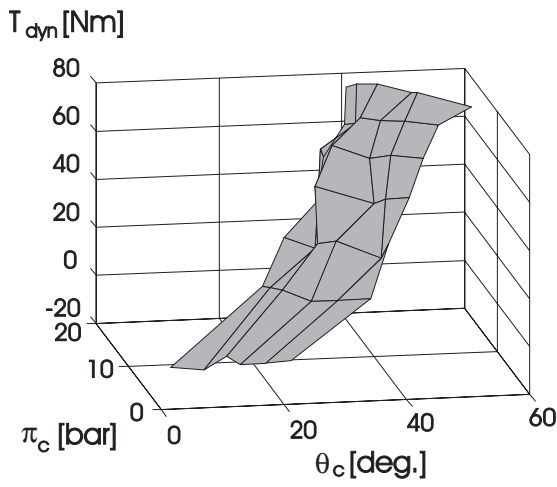


Figure 18: engine torque as a function of θ_c and π_c , 2500 rpm (compare to Figure 14)

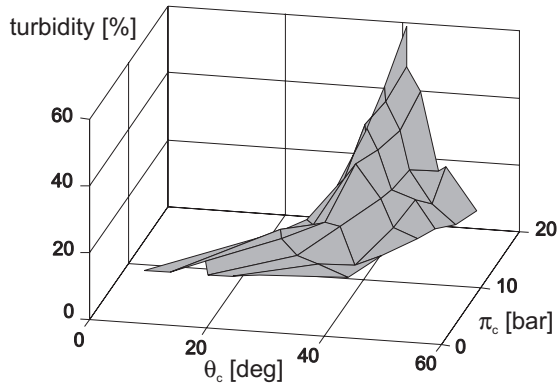


Figure 19: turbidity signal as a function of θ_c and π_c , 2500 rpm (compare to Figure 15)

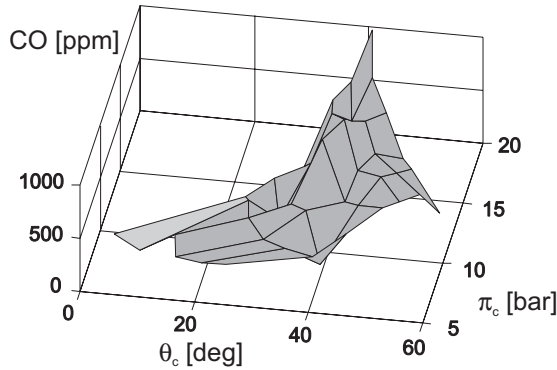


Figure 20: CO emissions as a function of θ_c and π_c , 2500 rpm (compare to Figure 16)

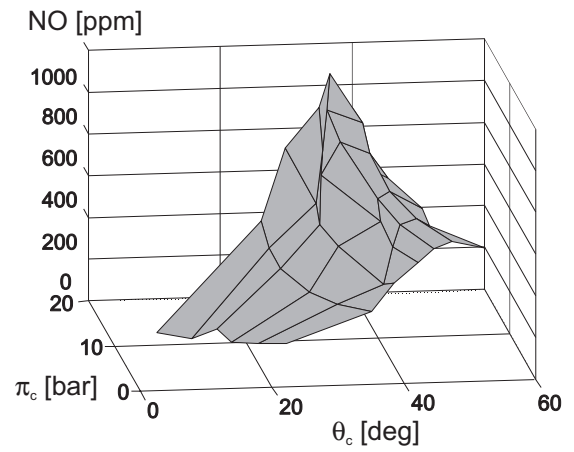


Figure 21: NO emissions as a function of θ_c and π_c , 2500 rpm (compare to Figure 17)

haust emissions are individual events without dynamics from rotation to rotation [22], it is possible to use Δp_{cyl} for feedforward control of the torque and the exhaust emissions. Therefore, a possible optimization criterion would be:

find (θ_c, π_c) which minimizes

$$V(\theta_c, \pi_c) = w_{turb} \cdot [turb] + w_{CO} \cdot [CO] + w_{NO_x} \cdot [NO_x] + w_{HC} \cdot [HC]$$

subject to

$$T_{dyn} = f(\theta_c, \pi_c) = T_{desired} \quad (16)$$

Here, w denotes arbitrary coefficients. Figure 9 gives the corresponding engine inputs, i.e. fuel mass m_F and injection angle θ_{IN} .

4.3 Ignition Control Using Adaptive Neural Networks

In SI engines, the objective of ignition control is to achieve optimum engine efficiency in the presence of changing engine and environmental conditions for each combustion event.

4.3.1 Control Architecture

In this application example, a combination of a linear feedback controller and an adaptive neural feed-forward structure has been employed for closed loop ignition control. In accordance to [2, 20], the control objective $MFB(9 \text{ deg}) = 0.5$ was selected, as this reference value results in optimum efficiency for SI engines, irrespectively of the operating point. Figure 22 shows the overall structure of the control system.

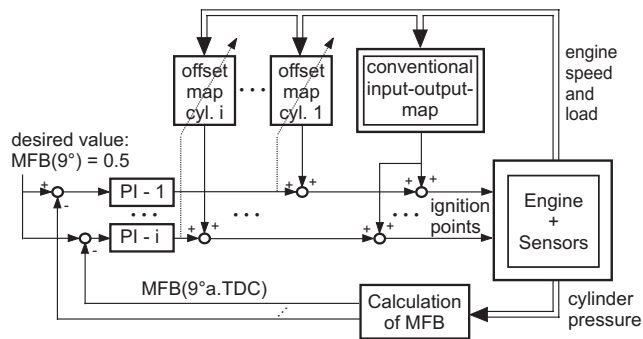


Figure 22: Structure of the ignition control system

In state-of-the-art open-loop control systems, an approximate value of the ignition points of all cylinders is basically determined by the engine load (a normalized value calculated from the intake manifold pressure signal) and the engine's rotational speed. This conventional input-output map is depicted on the upper right-hand side of Figure 22.

In a first step, this conventional feed-forward control system was improved by adding a linear feedback controller for each cylinder. These linear PI controllers modify the ignition point of the corresponding cylinder such that at a specified crank angle (9 deg after TDC) exactly 50 % of fuel is burned. An approximation for MFB has been derived by evaluating eq. (3) and (7).

These feedback controllers lead to good performance under steady state and slowly time variant operating conditions. However, they cannot be tuned with high gain. This is due to the fact

that after ignition of the air-fuel mixture, the subsequent combustion cannot be influenced any further. Therefore, ignition time can only be computed for the next cycle, based on the measurements from the present engine cycles. Thus, a dead time of one cycles is inherent. Moreover, as there exist significant cycle fluctuations even under steady operating conditions, the results of cylinder pressure evaluation of several engine cycles have to be averaged (a moving average over 10 cycles was used). Because the system error usually differs from one engine operating condition to another, during engine transients it takes a certain amount of time for the PI controller to "integrate" to a new ignition time.

To achieve high bandwidth control, the control system has been enhanced by adding an adaptive neural feedforward controller for each cylinder, which memorizes the appropriate offset values of the corresponding cylinder at the specific operating condition. The outputs of the linear controllers serve as reference signals for the adaptation of the adaptive RBF networks, as can be seen in Figure 22. The on-line learning is performed during regular operation of the engine as explained in Section 3.2.

During dynamic operation, all three components (the production look-up table, the PI-controllers and the neural net based offset look-up tables) are active.

4.3.2 Determination of the RBF Parameters

The RBF network has been used as a nonlinear feedforward correction of the linear PI feedback controller. This correction depends on the operating point defined by the engine load and the engine speed. Thus, the neural network operates on a two-dimensional input space. A clustering algorithm as mentioned in Section 3.2 was used to place the RBF centers \underline{c}_i in only those regions of the input space where data is present. The widths of the basis functions σ_i were determined using

a "nearest-neighbor" algorithm. Figure 23 shows the distribution of datapoints and the RBF centers obtained by k -means clustering in the input space for an exemplary test cycle.

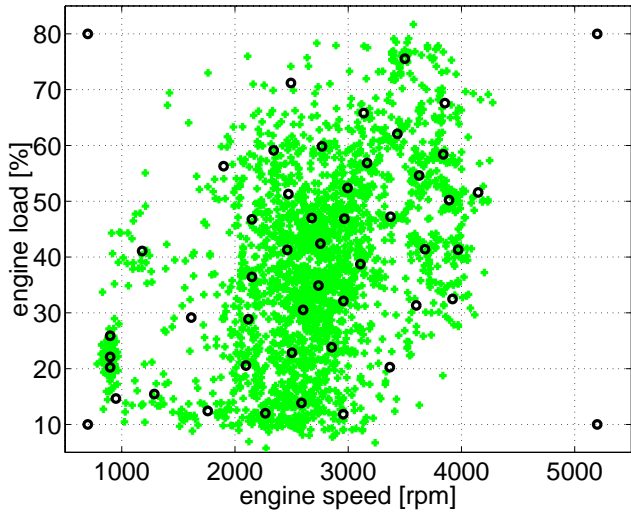


Figure 23: *Determination of centers of RBF-neurons by clustering*

The distribution of neurons in the input space was identical for all cylinders since beforehand no information concerning possible nonlinearities of the system are available. The positions of the neurons were held constant, only weight parameters have been adapted. Since this node distribution accounts for the data distribution during normal operation, "adaptation holes", i.e. areas of the input space where the network does not reflect the actual plant characteristics, are very unlikely to occur.

The weights w_i (here equivalent to the ignition timing offsets) of all interpolation nodes were set to zero initially and then adapted individually by applying the on-line training algorithm explained in 3.2. This algorithm adjusts the weights of the nodes according to the reference signal (output of the respective PI controller, cf. Figure 22). Since the adaptation is carried out locally, i.e. only the weights of the nodes which are activated at a certain operating point are modified, fast convergence is achieved.

4.3.3 Experimental Results

The control algorithm and cylinder pressure evaluation were implemented using C-code combined with MATLAB/SIMULINK. A rapid-prototyping system [9] was employed. A test vehicle equipped with a baseline engine, additional cylinder pressure sensors and a modified engine control unit, was used for the experiments. The developed controller worked at a sampling time of 5 ms.

After initialization of the network parameters, a 5-minute sequence of network training was performed during normal driving conditions. Figure 24 illustrates the resulting behavior for a fast change of the operating point. The upper diagram shows the engine load and speed. Starting from an engine speed of about 2200 rpm, after 15 s an acceleration takes place. The engine speed increases gradually and a pulse occurs in the engine load.

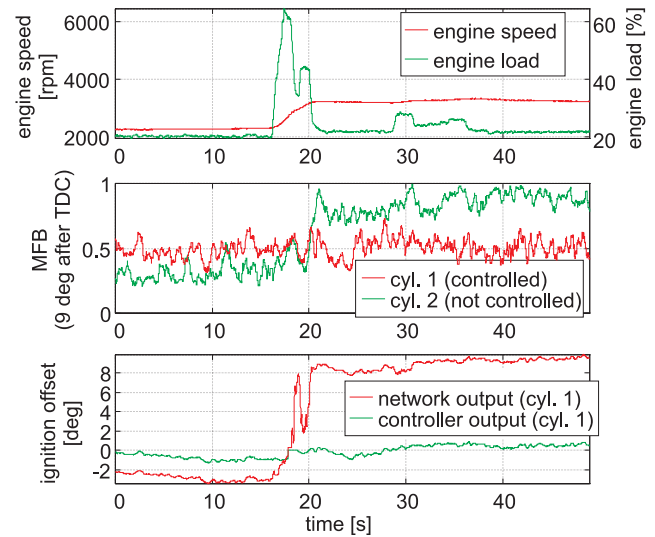


Figure 24: *Experimental results during a rapid change of the operating point (cyl. 1 with and cyl. 2 without the neural network control).*

The filtered MFB at 9 deg after TDC is shown in the second diagram for two different cylinders. Cylinder 1 is operated in closed-loop as described in Figure 22, whereas the ignition timing of cylinder 2 is solely determined by the conventional input-output map. For the controlled cylinder the

MFB at 9 deg. after TDC remains around 0.5, while the value of MFB for the second (uncontrolled) cylinder deviates from this optimal value.

The third diagram in Figure 24 shows, for cylinder 1, the output of the PI-controller and the network output. The network reacts immediately to the changing operation condition (feed-forward control). Since the weights of the network have already converged to their optimal values for the operating points that occur in this experiment, the output of the linear controller remains close to zero.

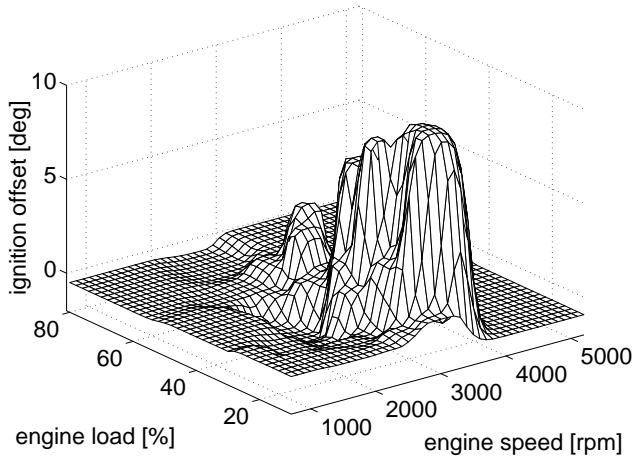


Figure 25: Ignition timing offsets represented by a RBF network (positive offset values imply a delayed ignition)

Unlike many other neural network type controllers, the parameters of the RBF based neural controller can be easily interpreted and supervised. For two-dimensional problems the parameters can be displayed as input-output map as it was done in Figure 25 for the ignition offset values of the RBF network as it was used for the test cycle in Figure 24. Obviously, for this cylinder a considerable offset is necessary in large parts of the operating domain, in order to optimize the ignition point. Unlike classical lattice-like input-output maps, the trained RBF network produces a smooth surface despite of considerable nonlinearities.

5 Conclusions

Various methods for feature extraction of the cylinder pressure signal have been proposed. A new method, the "difference pressure" signal, has been introduced. From Δp_{cyl} , it is possible to extract significant features that vary uniquely with the input signals. These features may be used for a neural network based supervision of the injection pump. Experimentally, the reconstruction of the input signals performed satisfactory in the stationary and in the dynamic case. In control engineering terms, the method may be viewed as a *dynamic engine observer* using internal states (the cylinder pressure) to estimate *inputs* (fuel mass and injection angle).

In addition, the unique relations between engine torque and exhaust emissions (*outputs*) and Δp_{cyl} (*internal states*) imply that the difference pressure signal carries the complete information of the torque production and the current exhaust emissions. This motivates feedforward control of the torque and exhaust emissions.

The demand for improved engine performance and efficiency has inspired the development of a closed-loop control system for ignition control based on the combustion pressure. Using cylinder-selective linear feedback controllers and neural adaptive feedforward controllers, the 50% point of energy conversion can be kept near to the optimal point in steady-state as well as under transient conditions. The proposed control system is capable to compensate for manufacturing tolerances, fuel quality variations and long-term effects such as aging or wear and tear of the engine. Moreover, the complexity and cost of engine calibration can thus be reduced dramatically.

In summary, employing real-time cylinder pressure information offers several advantages over conventional control strategies:

- improved engine diagnostics
- improved performance and greater fuel econ-

omy

- improved driveability
- reduced sensitivity to engine component manufacturing tolerances
- ability to adapt to engine wear and aging, as well as to changing environmental conditions and to variations in fuel quality
- emission reduction
- less calibration expense

References

- [1] C. Anastasia and G. Pestana. A cylinder pressure sensor for closed loop engine control. In *SAE Technical Paper Series*, number 870288, 1987.
- [2] M. Bargende. Most optimal location of 50 % mass fraction burned and automatic knock detection components for automatic optimization of si-engine calibrations. *MTZ Worldwide*, 56, 1995.
- [3] J. Bezdek. *Pattern Recognition with Fuzzy Objective Function Algorithms*. Plenum Press, New York, 1981.
- [4] M. Brown and C. Harris. *Neurofuzzy Adaptive Modelling and Control*. Prentice Hall, New York, 1994.
- [5] M. Brunt, H. Rai, and A. Emtage. The calculation of heat release energy from engine cylinder pressure data. In *SAE Technical Paper Series*, number 981052, 1998.
- [6] E. Gassenfeit and J. Powell. Algorithms for air-fuel ratio estimation using internal combustion engine cylinder pressure. In *SAE Technical Paper Series*, number 890300, 1989.
- [7] J. Gilkey and J. Powell. Fuel-air ratio determination from cylinder pressure time histories. *Journal of Dynamic Systems, Measurements, and Control*, 107:252–257, Dec. 1985.
- [8] I. Glaser and J. Powell. Optimal closed-loop spark control of an automotive engine. In *SAE Technical Paper Series*, number 810058, 1981.
- [9] H. Hanselmann. Automotive control: From concept to experiment to product. In *IEEE International Symposium on Computer-Aided Control System Design*, Sept. 1996.
- [10] M. Hart and M. Ziegler. Adaptive estimation of cylinder air mass using the combustion pressure. In *SAE Technical Paper Series*, number 980791, 1998.
- [11] W. Herden and M. Küsell. A new combustion pressure sensor for advanced engine management. In *SAE Technical Paper Series*, number 940379, 1994.
- [12] G. Hohenberg and I. Killmann. Basic findings obtained from measurement of the combustion process. In *Proceedings of the XIX Int. FISITA Congress*, number 82126, Melbourne, 1982.
- [13] M. Hubbard, P. Dobson, and J. Powell. Closed loop control of spark advance using a cylinder pressure sensor. *Journal of Dynamic Systems, Measurement, and Control*, pages 414–420, Dec. 1976.
- [14] T. Inoue, S. Matsushita, K. Nakanishi, and H. Okano. Toyota lean combustion system - the third generation system. In *SAE Technical Paper Series*, number 930873, 1993.
- [15] Y. Kawamura, M. Shinshi, H. Sato, N. Takahashi, and M. Iriyama. MBT control

- through individual cylinder pressure detection. In *SAE Technical Paper Series*, number 881779, 1988.
- [16] S. Leonhardt, C. Ludwig, and R. Schwarz. Real-time supervision for diesel engine injection. *Control Eng. Practice*, 3(7):1003–1010, 1995.
- [17] S. Leonhardt, C. Schmidt, K. Voigt, and R. Isermann. Real-time simulation of drive chains for use in dynamical engine test stands. *American Control Conference (ACC 92)*, 1992.
- [18] S. Leonhardt, R. Schwarz, and R. Isermann. Real-time supervision of the diesel engine injection process. In *SAE Technical Paper Series*, 1997.
- [19] R. Lippmann. An introduction to computing with neural nets. *IEEE ASSP Magazine*, (4):4–22, 1987.
- [20] F. A. Matekunas. Engine combustion control with ignition timing by pressure ratio management. *U.S. Patent*, 4,622,939, 1986.
- [21] J. Moody and C. J. Darken. Fast learning in networks of locally-tuned processing units. *Neural Computation*, 1(2):281–294, 1989.
- [22] E. Nitzschke. *Stationäre und instationäre Messung und Berechnung der Abgaszusammensetzung am Ottomotor*. PhD thesis, Technische Hochschule Darmstadt, 1992.
- [23] J. Powell. Engine control using cylinder pressure: Past, present, and future. *Journal of Dynamic Systems, Measurement, and Control*, 115:343–350, 1993.
- [24] K. Sawamoto, Y. Kawamura, T. Kita, and K. Matsushita. Individual cylinder knock control by detecting cylinder pressure. In *SAE Technical Paper Series*, number 871911, 1987.
- [25] H. Werntges. Partitions of unity improve neural function approximators. In *IEEE International Conference on Neural Networks (ICNN)*, volume 2, pages 914–918, San Francisco, USA, 1993.